Received: 17 March 2021 | Revised: 16 July 2021 | Accepted: 18 October 2021

DOI: 10.1002/hbm.25698

RESEARCH ARTICLE

WILEY

Contribution of the multi-echo approach in accelerated functional magnetic resonance imaging multiband acquisition

Anežka Kovářová[1,2] | Martin Gajdoš[1] | Ivan Rektor[1,2] | Michal Mikl[1]

[1]CEITEC – Central European Institute of Technology, Masaryk University, Brno, Czech Republic

[2]First Department of Neurology, Faculty of Medicine of the Masaryk University, Brno, Czech Republic

Correspondence
Michal Mikl, CEITEC – Central European Institute of Technology, Masaryk University, Kamenice 5, Brno 625 00, Czech Republic.
Email: michal.mikl@ceitec.muni.cz

Funding information
Ministerstvo Školství, Mládeže a Tělovýchovy, Grant/Award Numbers: CZ.02.1.01/0.0/0.0/16_013/0001775, LM2015062, LM2018129; European Regional Development Fund

Abstract

We wanted to verify the effect of combining multi-echo (ME) functional magnetic resonance imaging (fMRI) with slice acceleration in simultaneous multi-slice acquisition. The aim was to shed light on the benefits of multiple echoes for various acquisition settings, especially for levels of slice acceleration and flip angle. Whole-brain ME fMRI data were obtained from 26 healthy volunteers (using three echoes; seven runs with slice acceleration 1, 4, 6, and 8; and two different flip angles for each of the first three acceleration factors) and processed as single-echo (SE) data and ME data based on optimal combinations weighted by the contrast-to-noise ratio. Global metrics (temporal signal-to-noise ratio, signal-to-noise separation, number of active voxels, etc.) and local characteristics in regions of interest were used to evaluate SE and ME data. ME results outperformed SE results in all runs; the differences became more apparent for higher acceleration, where a significant decrease in data quality is observed. ME fMRI can improve the observed data quality metrics over SE fMRI for a wide range of accelerated fMRI acquisitions.

KEYWORDS
acquisition acceleration, BOLD, multi-echo fMRI, simultaneous multi-slice imaging, TE dependence

1 | INTRODUCTION

Functional magnetic resonance imaging (fMRI) is a well-established method for noninvasive brain mapping. The detection of brain activation is typically based on changes in blood-oxygen-level-dependent (BOLD) images, that is, changes in the transverse relaxation rate or R_2^* due to different blood oxygenation levels (Ogawa, Lee, Kay, & Tank, 1990). The method commonly used for fMRI data acquisition is echo-planar imaging (EPI). At a 3 mm resolution, it is possible to scan the whole brain using a standard EPI sequence in about 2–4 s. This repetition time (TR) is not able to efficiently and precisely sample hemodynamic responses. The EPI method provides a relatively meaningful trade-off between spatial and temporal resolutions. But for higher spatial resolutions or fast sampling with whole-brain coverage, combinations of EPI with various acceleration techniques are required. The first group of techniques allows the acceleration of acquisition by using a reduced amount of k-space rows (SENSitivity Encoding [SENSE] or GeneRalized Autocalibrating Partial Parallel Acquisition [GRAPPA]; Griswold et al., 2002; Pruessmann, Weiger, Scheidegger, & Boesiger, 1999); the second group accelerates the acquisition by exciting several slices simultaneously and then decoding this image information; this is called the simultaneous multi-slice (SMS) technique or multiband (MB) technique because several slices are being excited with multiple radiofrequency bands (Feinberg & Setsompop, 2013). Both acceleration techniques can be combined. The biggest contributions of the SMS/MB techniques

(hereafter, we use the terms SMS and MB as equivalent) are reduced acquisition times and increased temporal and/or spatial resolution (Setsompop et al., 2012), (Chen et al., 2015). The BOLD contrast-to-noise ratio (CNR) increases with the square root of the number of slices (Hamilton, Franson, & Seiberlich, 2017). SMS methods can provide better time resolutions and possibly higher CNR values, depending on the MB factor and the defined CNR metric, for fMRI experiments than conventional acquisitions. Todd et al. (2016) proved that using an MB factor higher than 2 produces significant improvements in BOLD sensitivity using a 3T scanner as compared to unaccelerated sequences for motor and visual tasks. Another 3T MB EPI study showed significant increases in BOLD activation for fast-event-related tasks (Demetriou et al., 2018).

It is known that fMRI data can be seriously affected by various types of artifacts, including head motion and physiological and hardware-induced artifacts (Power, Barnes, Snyder, Schlaggar, & Petersen, 2012). Despite advances in hardware and acquisition techniques, the optimization of fMRI acquisition protocol (selection of optimal TR, echo time (TE), flip angle, level of acceleration, spatial resolution, etc.) as well as the optimization of data processing are still important issues. Classic EPI sequences acquire data at one TE selected in order to obtain the optimal contrast (Triantafyllou, Wald, & Hoge, 2011). With 3T MR scanners, the TE value is usually in the range of 30–40 ms (Triantafyllou et al., 2011). However, in some brain areas the optimal TE can vary according to the T2* of the specific tissue, which may lead to lower sensitivity. Higher TE brings higher BOLD percent signal changes; at the same time, various brain regions are more affected by susceptibility artifacts. This issue can be solved with ME acquisition, when three or more echoes are measured within one TR interval. For instance, Kundu et al. (2017) reported using a ME fMRI approach with three different TEs (Kundu et al., 2017). With three echoes, the value of the first TE is typically selected to be as short as possible while maintaining the other acquisition parameters (e.g., 15 ms; Kundu, Inati, Evans, Luh, & Bandettini, 2012). The other two TE are then as close as possible given the capabilities of the device. The earliest TE has the highest signal intensity but lower levels of contrast between gray and white matter and cerebrospinal fluid. Higher TEs provide less MRI signal but higher BOLD differences between two brain activation states (i.e., differences in T2*), and these echoes are more sensitive to susceptibility artifacts (Kundu et al., 2017). One advantage of the ME approach is the possibility to model the signal drop associated with the T2* for each voxel. This makes it possible to better understand the formation of individual signals and subsequently suppress undesirable artifacts (Posse et al., 1999). Individual echoes are typically combined to one optimally-combined BOLD series, weighted by voxelwise CNR (Poser, Versluis, Hoogduin, & Norris, 2006). The ME approach was also proven to alleviate problems with signal loss in brain areas prone to susceptibility artifacts and signal dropouts (Fernandez, Leuchs, Sämann, Czisch, & Spoormaker, 2017; Kundu et al., 2013; Posse et al., 1999). A study by Fernandez et al. (2017) showed that ME EPI yielded better results at detecting task activation in the ventromedial prefrontal cortex than standard single-echo EPI, which had signal loss due to macroscopic field inhomogeneity.

The use of ME EPI together with MB EPI (MEMB EPI) thus exploits both the possibility of fast acquisition and the robustness of ME EPI against signal drop caused by susceptible artifacts and CNR optimization. Our goals are to achieve a compromise between the quality of the data collected and the speed of acquisition, to determine the contributions of ME to different levels of acceleration, and to compare them with classical EPI. This should be useful to researchers for many applications. Faster acquisitions can provide higher statistical values due to the increase of available observations and the better sampling of noise artifacts.

Few studies and experiments have combined the ME and MB approaches. A few 7T studies used ME EPI together with MB for fMRI experiments to obtain the best features of both approaches. For example, a comparison of data from the basal ganglia acquired using a 7T scanner by Puckett et al. (2018) demonstrated MEMB outperforming single-echo multi-band (SEMB) in image quality and functional contrast (Puckett et al., 2018). Boyacioğlu, Schulz, Koopmans, Barth, and Norris (2015) studied MEMB compared to unaccelerated ME at 7T. Their findings suggest that MEMB provides better results in terms of sensitivity and the correct detection of activation clusters than ME single-band EPI at high field strengths. On the other hand, high field strength caused an increase in susceptibility artifacts and different signal characteristics; other studies using a 3T scanner have thus been conducted. In one study, Olafsson, Kundu, Wong, Bandettini, and Liu (2015) compared MEMB and single-band ME acquisitions and demonstrated that significantly more BOLD components from ME-ICA were found using MEMB-EPI data than ME-EPI data. They explained that these results were caused by both the increased number of temporal samples and the enhanced ability to filter out high-frequency artifacts. Amemiya, Yamashita, Takao, and Abe (2019) demonstrated that ME improved language mapping and laterality identification using combined MEMB data compared to a single-echo data from the same MEMB acquisition (Amemiya et al., 2019). Cohen, Nencka, Marc Lebel, and Wang (2017) used a MEMB pseudo-continuous arterial spin labeling (pCASL) sequence with and without ME-ICA and compared it to a single-TE-series from the same sequence; the results showed that MEMB yields higher connectivity and extent. Cohen et al. (2020) recently published two more papers on MEMB. In 2020, they explored task fMRI activation using MEMB and found that it showed higher activation volume and higher sensitivity than SEMB without losing specificity. Their most recent study, published in 2021, stated that all seed-based resting-state functional connectivity and functional connectivity density were significantly higher for MEMB than for SEMB. The results indicated that MEMB was a promising technique for resting-state fMRI usage (Cohen, Yang, Fernandez, Banerjee, & Wang, 2021). The two articles by Cohen et al. had only two acquisition schemes (with and without MB acceleration); therefore, the effects of various slice accelerations were not evaluated in detail. Cohen et al. used different runs for SE and ME acquisition. In general, this makes it possible to optimize acquisition for both approaches. On the other hand, results can be

affected by potential effects of learning, habituation, boredom, and so on if the study is not well balanced and designed to avoid these confounding factors. In our study, we chose a different approach—SE data were taken as the middle echo from ME acquisition. This makes it possible to compare the exact same neural responses. However, SE data cannot be fully optimized in this approach—mainly, the TR is slightly longer (about 20%) than in independent runs with standalone SE acquisition.

A side effect of using accelerated fMRI acquisition is the necessity to use lower flip angles to avoid T1-modulaton within the BOLD time-series in gray matter. Acquisition with lower flip angles produces fewer measured signals, which affects the image quality. This should not affect the percent signal change of the BOLD response; on the contrary, it can help to decrease the amount of physiological artifacts in the BOLD time-series (Gonzalez-Castillo, Roopchansingh, Bandettini, & Bodurka, 2011). A study by Gonzalez-Castillo et al. (2011) evaluated SE data without slice acceleration. For this reason, we added runs with different flip angles as another factor to different slice acceleration levels.

In our study, we tried to evaluate extensively the advantages of ME acquisition for various acquisition settings, especially for various levels of slice acceleration, with a range of metrics assessing data quality and activation results. The use of more metrics can provide a more comprehensive view of the problem of optimizing the measuring and processing of fMRI data because different metrics are sensitive to different aspects of data quality and/or detection ability to the effect of interest in our data (i.e., different neuroscience hypotheses and goals of neuroimaging studies). For this reason, we combined metrics based on classical fMRI task activation analysis (e.g., number of active voxels, t-values in regions of interest (ROIs), residuals from general linear model fitting); temporal signal-to-noise ratio (tSNR) in modification for the Human Connectome Project (Smith et al., 2013); signal-to-noise separation (SNS) as introduced by Shirer, Jiang, Price, Ng, and Greicius (2015); and data smoothness and global metrics from graph connectivity analysis.

2 | METHODS

Data were collected from 26 healthy volunteers ages 20–38; 9 women and 17 men. Exclusion criteria were any neurological, psychiatric, or mental disorder. All participants were thoroughly familiar with the complete contents of the measurement, were informed about safety, and signed informed consent forms. The study protocol was approved by the Masaryk University Ethics Committee. The measurements were performed on the Siemens Prisma 3T MR whole-body scanner with 64-channel head-neck coil in the Laboratory of Multimodal and Functional Imaging at CEITEC Masaryk University.

The protocol for all measurements contained seven MB EPI fMRI runs with different levels of acceleration (different MB factor values), TR, and flip angles. The parameters of the runs are shown in Table 1 for clarity. First, high-resolution anatomical images T1-MPRAGE were scanned for each subject and were later used for more accurate localization of the active areas of the brain and for detecting any possible abnormalities that could result in a subject's removal from the study. In the second part of the protocol, we acquired the seven BOLD runs with different acquisition parameters. fMRI protocols were based on the MB-EPI BOLD sequence obtained from the Centre for Magnetic Resonance Research, University of Minnesota. The acquisition time of each run was 6 min, but different numbers of images were obtained in each run due to different TR values. Both field of view (FOV) (192 × 192 mm) and TE (17.00, 34.64, and 52.28 ms) were constant for all fMRI runs. TE values were chosen according to the MR machine and sequence capabilities, as well as according to recommendations in ME EPI review articles (Gonzalez-Castillo et al., 2011, 2016; Kundu et al., 2012, 2017).

The first TE was chosen approximately as the lowest possible value (rounded up to an integer), the second TE was as close as possible to the first one and was very similar to the typical optimal TE used in SE acquisition, and the third TE was as close as possible to the second one (to not unnecessarily prolong the TR). Flip angles were based on the Ernst angle calculation and slightly rounded down. In addition to this standard flip angle, we used the flip angle from the next acceleration level (i.e., 45° in run 2 to be identical to run 3). The measurements of runs 1–7 were counterbalanced to avoid the effect of order.

The fMRI task was a block-design task that consisted of two regularly alternating epochs. The first epoch was at baseline with instructions to lie still and fix the eyes on a red cross on a black background in the middle of the stimulation screen. Additionally, subjects were instructed not to think intensely. This epoch lasted 30.25 s. A second epoch followed in which the red numbers 1, 2, 3, 4 in a series of 10 gradually appeared on the checkerboard background and the

TABLE 1 Acquisition parameters for individual runs

fMRI run	Number of scans	Resolution (mm)	PAT factor	MB factor	TR (ms)	Flip angle (°)	Acq. matrix	No. of slices
Run 1	120	3 × 3 × 3.5	2	1	3,050	80	64 × 64	48
Run 2	120	3 × 3 × 3.5	2	1	3,050	45	64 × 64	48
Run 3	450	3 × 3 × 3.5	2	4	800	45	64 × 64	48
Run 4	450	3 × 3 × 3.5	2	4	800	20	64 × 64	48
Run 5	600	3 × 3 × 3.5	2	6	600	45	64 × 64	48
Run 6	600	3 × 3 × 3.5	2	6	600	20	64 × 64	48
Run 7	900	3 × 3 × 3.5	2	8	400	20	64 × 64	48

subject was supposed to press the corresponding buttons simultaneously. This active measurement period lasted 21.35 s, and the sequence of the two epochs was repeated eight times within one fMRI run.

2.1 | Preprocessing

The obtained data was processed using the toolbox SPM12 (rel. num. 6225) implemented in MATLAB. For each run, the images were aligned using the SPM12 realign procedure in the following manner: all images of the middle echo were realigned to the first image of the second echo; subsequently the same translations and rotations were applied to align the first and third echoes. Composite ME data were calculated using the contrast-to-noise weighted average. Thus, in each voxel, three temporal SNR (tSNR) values were calculated, one for each TE, and the resulting voxel value was given by the weighted average of the three original tSNR-weighted values and TEs. The tSNR-weighted model was chosen with reference to the recommendations of (Poser et al., 2006), who experimentally demonstrated that ME tSNR-weighted data provided better sensitivity than conventional processing techniques such as simple summation.

The presence of dropouts and spatial abnormalities in the data was checked with the mask explorer tool (Gajdoš, Mikl, & Mareček, 2016). The data quality, with respect to presence of excessive movement, was inspected with the movement_info tool (available at https://www.nitrc.org/projects/movement_info/) exploiting framewise displacement (FD) measures (Power et al., 2012). The data was controlled for number of scans per subject exceeding FD 0.5 mm and 1.5 mm. When using the thresholds of 20% of scans exceeding FD = 0.5 mm (as in e.g., Šimko, Pupíková, Gajdoš, & Rektorová, 2021) and 1% of scans exceeding FD = 1.5 mm, all of the participants were eligible. For details on the presence of movement in the data, see Table S1 in the Supporting Information.

In the next step, the rest of the standard preprocessing of the optimally combined ME data was performed using the SPM12 toolbox. Co-registration to the anatomical images was done within all sequences of all subjects. Anatomical and functional images were subjected to spatial normalization to the Montreal Neurological Institute template. Normalized data were then spatially smoothed using a 5 mm Full Width at Half Maximum Gaussian filter.

The middle TE (~35 ms) was chosen for the SE data as it is within the recommended TE value range (Triantafyllou et al., 2011). Thereafter, spatial normalization and spatial smoothing of functional data was performed (Figure 1).

Single-subject-level statistical analysis was performed using a general linear model (GLM) as implemented in SPM12. One model was estimated using data from the middle echo; the other model was based on optimally combined ME data. The GLM design matrix consisted of 26 regressors: the response to experimental stimulation, 24 movement regressors (Friston, Williams, Howard, Frackowiak, & Turner, 1996), and the constant term. An autoregression model in SPM was used with the AR (fast) option to take into account the different order of autocorrelation in different fMRI sampling rates (McDowell & Carmichael, 2019; Sahib et al., 2016).

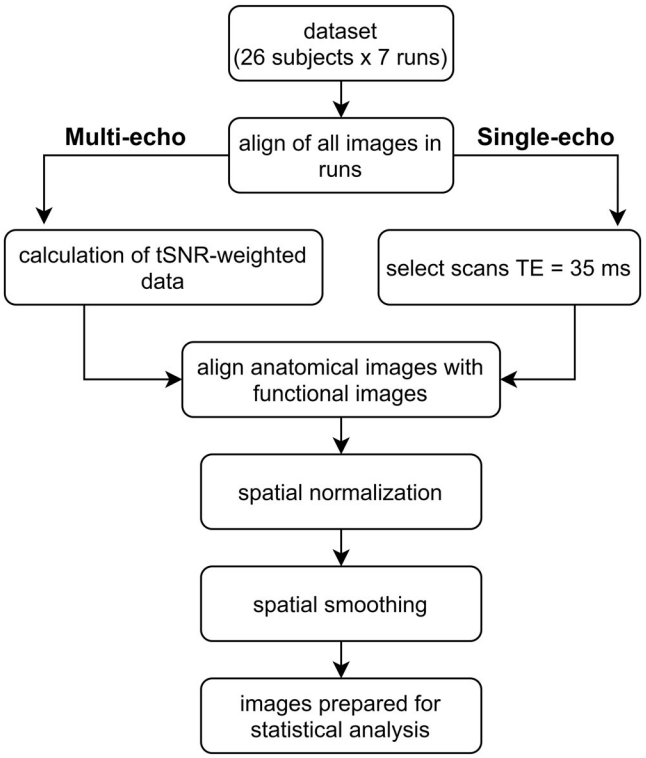

FIGURE 1 Scheme of data preprocessing

This was followed by a group analysis in which the SE and ME statistical models of the individual subjects were assessed with random effect statistical model.

2.2 | Global metrics

We used several data metrics to evaluate the quality of preprocessed data; that is, the metrics were calculated on preprocessed data before the GLM estimation or the metrics were based on subsequent GLM results. The tSNR metric (Krüger & Glover, 2001) was modified according to Smith et al. (2013). The calculated tSNR value (mean of individual time-series divided by standard deviation [*SD*]) was multiplied by the square root of the number of scans; we used the abbreviation tSNRn for clarity. The statistical power of such a large number of timepoints should balance the SNR drop in the images. tSNRn was calculated in each voxel and subsequently averaged over the defined region—for global metrics, over the entire gray matter or white matter.

Another global metric, SNS (Shirer et al., 2015), evaluates the distance (with *t*-value of two-sample *t*-test) between correlations of anatomical areas of the brain to random correlations with noise signals; that is, SNS evaluates the ability to evaluate functional connectivity. The global effect of data on functional connectivity can be assessed with graph metrics. We chose path length and node strength because

a previous study (Gajdoš, Výtvarová, Fousek, Lamoš, & Mikl, 2018) showed that these two metrics were clearly disturbed from the basic level by noisy data. Decreasing node strength and increasing path length cause the network to become more random. These metrics were calculated using the Brain Connectivity Toolbox and were based on functional connectivity matrices created with brain parcellation using the Automated Anatomical Labeling (AAL) atlas (Tzourio-Mazoyer et al., 2002) with 116 ROIs.

We calculated the number of active voxels (using p <.05 FWE corrected) and the sum of residual mean squares from GLM activation models averaged over gray matter as global metrics. Another global metric used in this study was spatial smoothness of the data, used in the quality control pipeline in the Human Connectome Project (Marcus et al., 2013).

The metrics described above were subsequently analyzed in statistical software SPSS 27 using generalized mixed models with factors: SE/ME version of data (SE or ME), acceleration factors (MB1, MB4, MB6, and MB8), and flip angles (higher or lower in the same acceleration level). This enabled the evaluation of the general effects of ME data, acceleration, and decreased flip angles on the data. To evaluate individual differences between SE and ME and between standard and decreased flip angles, we calculated paired t-tests. A p-value of .05 corrected for multiple comparison was used to assess significance. Moreover, the difference between SE and ME models was expressed as a percent change in the observed metrics for better interpretation and quantification of this effect.

2.3 | Evaluation of selected ROIs

To evaluate the resulting statistical images and other parameters, 10 ROIs were selected from all AAL regions (Tzourio-Mazoyer et al., 2002) based on their relevance for the activation of our fMRI task and spread across different parts of brain. An overview of the selected regions is presented in Table 2.

In addition, β weights, residues, t-values, percentage signal change (PSC; Luo & Nichols, 2003), and task-based SNR (amplitude of fitted BOLD response divided by *SD* of residuals) were calculated across all subjects, sequences, and ROIs. *T*-values within each ROI were sorted by size, and the 50 largest ones in each ROI were selected for further evaluation. Moreover, the positions of these top 50 were stored for all of the above metrics. All results were finally stored in a separate structure.

The average correlation of individual voxel time-series with a representative signal in ROI represents the homogeneity of the voxel data contained in each ROI. The representative signal in a particular ROI was calculated as a mean of all individual time-series. The correlation of all voxels in ROI with this representative was then calculated. The resulting value of the average correlation of the representative signal in the ROI was determined across the correlations in all voxels. A higher value represents better area homogeneity in the data.

The number of suprathreshold voxels was calculated in all ROIs for each sequence, across all subjects within the SE and ME first-level models. It is the number of suprathreshold voxels in a certain ROI; the threshold was calculated on the FWE-corrected significance level of $p = .05$.

PSC provides information on the BOLD contrast caused by a change in the ratio of oxyhemoglobin to deoxyhemoglobin in passive and active states. PSC was calculated as in Luo and Nichols (2003), individually in each voxel and then an average was performed for the whole ROI or a selected subset of 50 voxels with the strongest statistic power.

The ROI metrics described above were subsequently analyzed in statistical software SPSS 27 using generalized mixed models in a similar way as the global metrics. The following factors were used in the statistical models: SE/ME data (SE or ME), acceleration factors (MB1, MB4, MB6, and MB8), flip angles (higher or lower in the same acceleration level), and ROI_ID (1–10). This enabled the evaluation of the general effects of ME data, acceleration, decreased flip angles, and individual ROI on the data. To evaluate individual differences between

TABLE 2 Overview of selected AAL regions for ROI metrics

ROI_ID	ROI description	AAL index	Mean cover—SE model	Mean cover—ME model
1	Left precentral gyrus (L PCG)	2	91.3%	91.7%
2	Left supplementary motor area (L SMA)	19	97.1%	97.7%
3	Right supplementary motor area (R SMA)	20	98.5%	99.0%
4	Left calcarine	43	96.8%	97.7%
5	Right calcarine	44	99.4%	99.6%
6	Left middle occipital gyrus (L MOG)	51	96.4%	96.8%
7	Right middle occipital gyrus (R MOG)	52	90.4%	91.0%
8	Left postcentral gyrus (L PCG)	57	94.8%	94.9%
9	Left pallidum	75	100%	100%
10	Right pallidum	76	100%	100%

Note: Mean cover represents the arithmetic mean of the covers of regions with valid voxels across all subjects. It is expressed as a percentage of all voxels in the AAL regions covered with data in the SPM mask. Voxels with a BOLD signal higher than 80% of the mean signal are marked 1 in the SPM mask, and only these voxels are used for subsequent analyses.

SE and ME and between standard and decreased flip angles, we calculated paired *t*-tests. A *p*-value of .05 corrected for multiple comparison was used to assess significance. Moreover, the difference between SE and ME data was expressed as a percent change in observed metrics for better interpretation and quantification of this effect.

3 | RESULTS

The greatest activation was observed, as expected, in the visual cortex and motor areas (especially in the left hemisphere). When comparing SE data and ME data (see Figure 2), there are only minor differences in group activation maps. ME data provide a slight increase in the number of active voxels and *t*-values. The group activation maps have rather illustrative purpose because our main results are based on global and local metrics.

3.1 | Global metrics

The distributions of global metrics are shown in Figure 3. Relative changes in the ME results with respect to the SE are shown in Figure 4. Figure 5 is a visualization of the effects of several factors and interactions from the generalized mixed model calculated by SPSS software. The significance of all the factors and interactions is presented in Table 3. There is a significant effect of the factor ME (SE vs. ME data) in all the observed global metrics. The ME data provides higher tSNRn both in gray matter and white matter (ranging from 15 to 70% according to the acquisition parameters), higher SNS (from 7 to 19%), more suprathreshold voxels (from 9 to 67%), higher smoothness of data (from 1 to 9%), lower residuals (from 26 to 67%), lower path length (from 5 to 25%), and higher node strength (from 1 to 50%). All metrics are affected by different MB factors (i.e., acceleration of acquisition). But while a higher MB factor caused a monotonic decrease in some metrics (tSNRn in white matter; SNS;

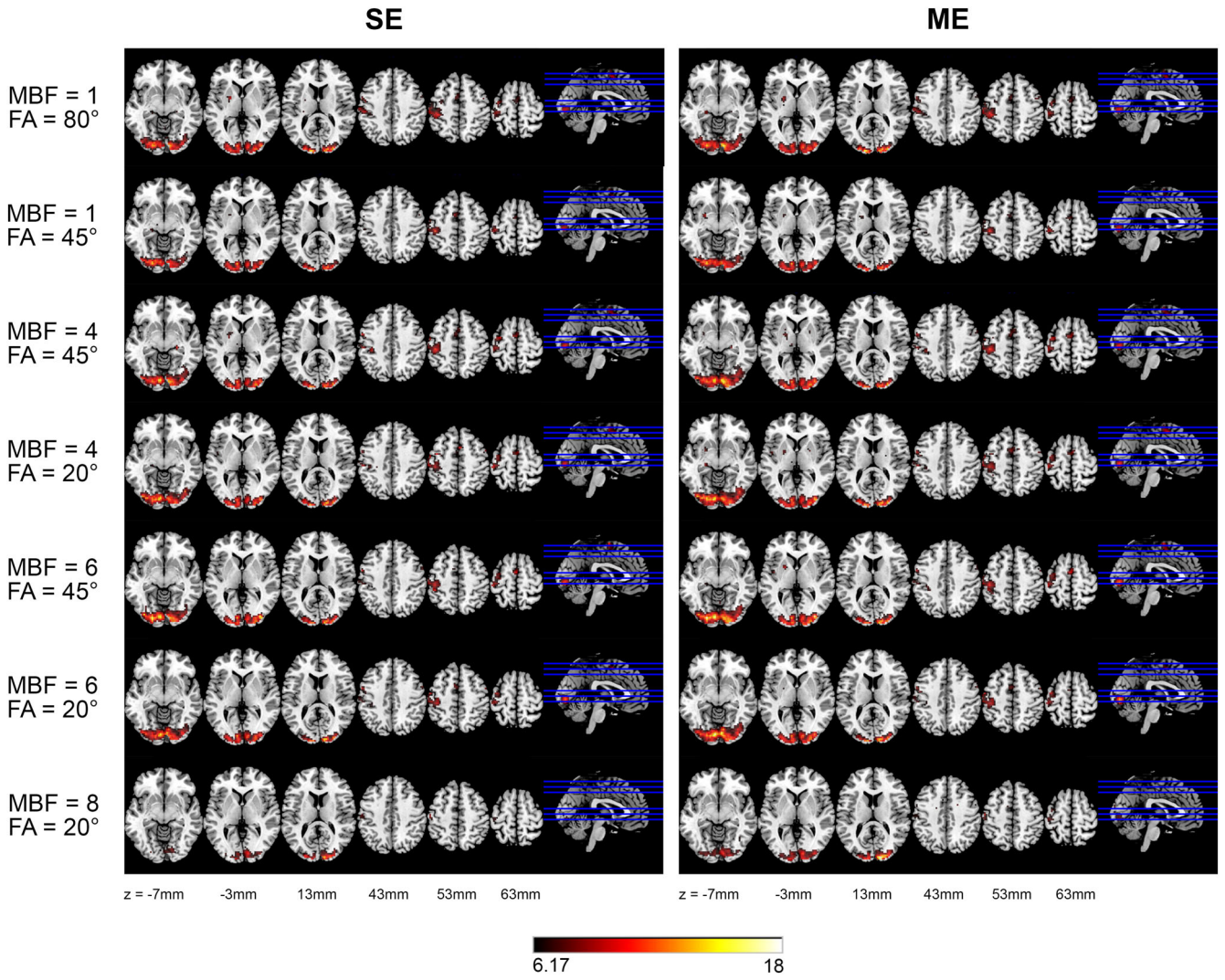

FIGURE 2 Example of group activation maps comparing SE and ME data. Runs 1–7 are presented as rows. Multi-band factors and flip angles are depicted on the left side for each functional run. Activation map's threshold was $p < .05$ FWE corrected and this corresponds to $t > 6.17$. FA, flip angle; MBF, multi-band factor; ME, optimally combined multi-echo data; SE, single echo data

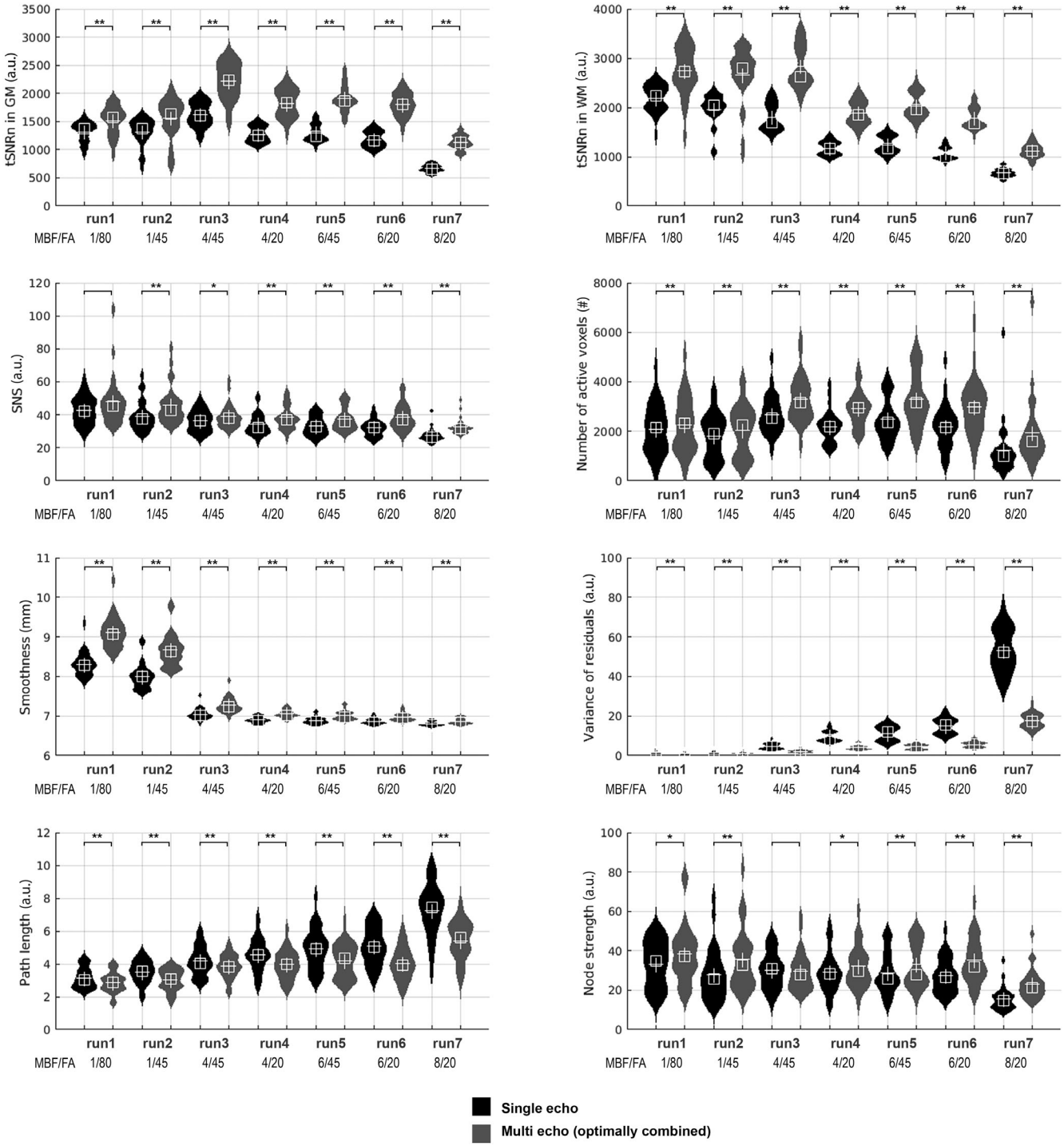

FIGURE 3 Distribution plots of global metrics for SE (black) and ME data (gray). White box represent median, white cross represents the mean of the distribution. Multi-band factors and flip angle values are given under the *x*-axis for each run. Significance of post-hot test (comparing SE and ME data from the same run) is depicted with stars above the distribution plots. * corresponds to p <.05 uncorrected. ** corresponds to p <.05 corrected for number of runs. FA, flip angle; GM, gray matter; MBF, multi-band factor; ME, optimally combined multi-echo data; SE, single echo data; WM, white matter

smoothness), and a monotonic increase in others (residuals, path length), there were also metrics with more complex behavior. Specifically, in the tSNRn in gray matter and the number of suprathreshold voxels, MB factors of 4 and 6 provided higher or equal values to the MB factor of 1 (data without slice acceleration), and the MB factor of 8 provided the lowest values. The lower flip angle affected only some metrics (see Table 3 for details) and only residuals were affected by interactions between the ME/SE model and flip angle. This means that the flip angle did not have a significant impact on data quality improvements caused with the ME data. On the other hand,

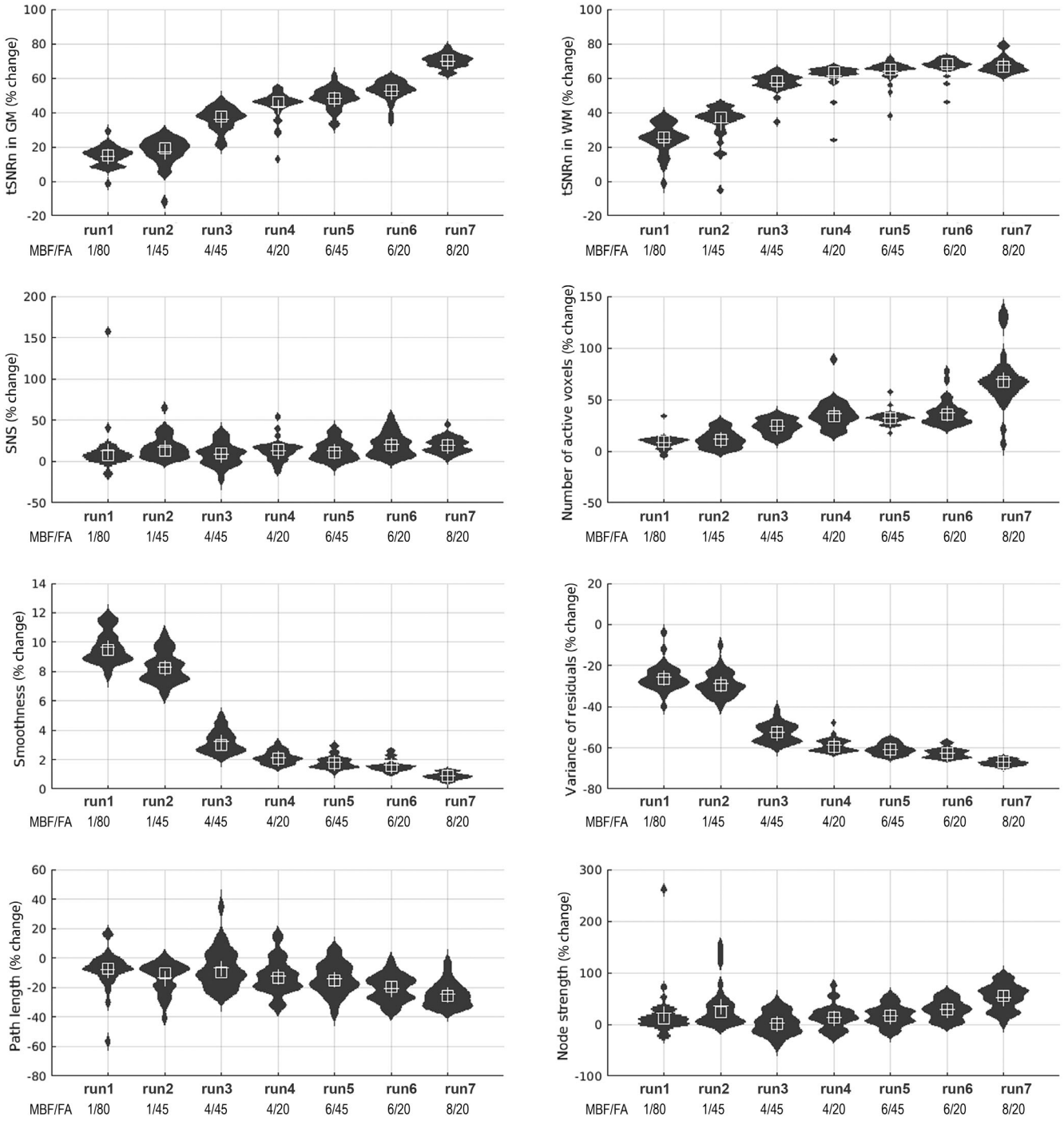

FIGURE 4 Distribution plots of the percent change between SE and ME global metrics (positive number corresponds to increase of metric for ME data). White box represent median, white cross represents the mean of the distribution. Multi-band factors and flip angle values are given under the *x*-axis for each run. FA, flip angle; GM, gray matter; MBF, multi-band factor; ME, optimally combined multi-echo data; SE, single echo data; WM, white matter

interactions between the ME/SE factor and MB factor were significant in a majority of metrics (all except SNS, path length, and node strength). Practically, this means that the ME data provided greater benefits for higher acceleration factors (see the percent effect sizes in Figure 4 for details). The effects of flip angles on global metrics (percent effect of decreased flip angle together with *p*-value of post-hoc test) are presented in Table S2.

3.2 | Analysis of ROIs

One known benefit of ME data is a lower sensitivity to signal dropouts, that is, better coverage of a standard brain template with valid data. This effect is visible for eight regions in Table 2. Two regions are fully covered both in SE and ME data. Even if the changes in cover between the SE and ME data are small, the statistical effect evaluated

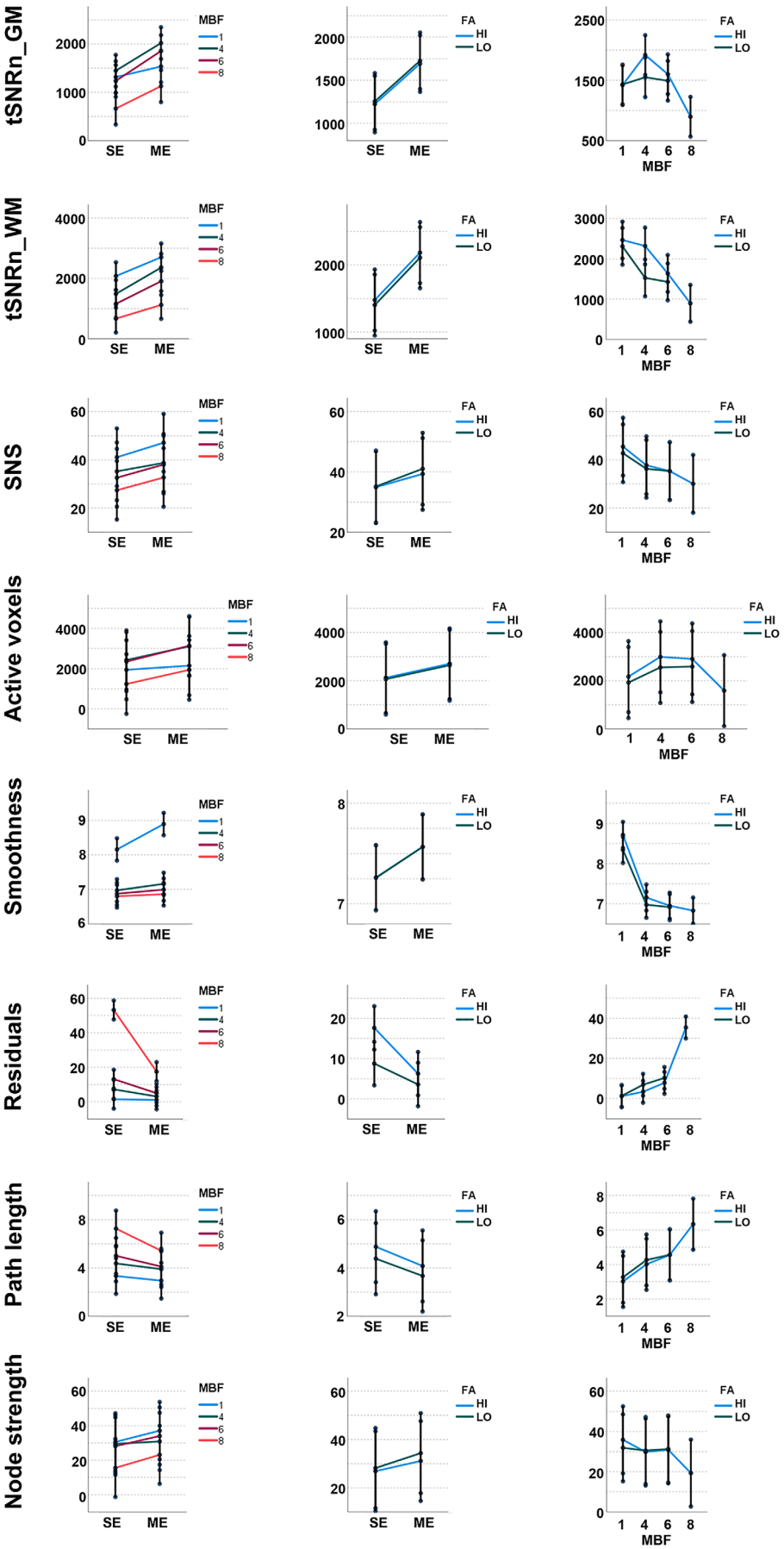

FIGURE 5 Overview of the effect of modeled factors in generalized mixed model statistics for global metrics. Each row represents one metric (depicted on the left side). Estimated means (dots connected with lines) and 95% confidence intervals (whiskers) are presented for three types of graphs. First shows the effect of ME data on the metric for individual multi-band factors. Second shows the effect of ME data on the metric for two levels of flip angles (high or low angle). Third type shows the effect of multi-band factor on the metric for two levels of flip angles. FA, flip angle; GM, gray matter; MBF, multi-band factor; ME, optimally combined multi-echo data; SE, single echo data; WM, white matter

TABLE 3 Results from generalized mixed effect models assessing the factors of SE versus ME, slice accelerations (MB factor), and flip angles (higher vs. lower)

Metric	Signific. of factor ME	Signific. of factor MBF	Signific. of factor FA	Signific. of interaction ME × MBF	Signific. of interaction ME × FA	Signific. of interaction MBF × FA
tSNRn GM	<.001	<.001	<.001	<.001	.976	<.001
tSNRn WM	<.001	<.001	<.001	<.001	.096	<.001
SNS	<.001	<.001	.078	.534	.254	.362
Active voxels	<.001	<.001	<.001	.019	.832	.633
Smoothness	<.001	<.001	<.001	<.001	.052	<.001
Residuals	<.001	<.001	<.001	<.001	.007	.001
Path length	<.001	<.001	.079	<.001	.164	.477
Node strength	<.001	<.001	.388	.098	.160	.151

Note: The values in the table represent the significance (p-value) of each individual factor or interaction between factors for each global metric. Abbreviations used in the table: FA, flip angle; ME, multi-echo; MBF, multiband factor; SNS, signal-to-noise separation; tSNRn, temporal signal-to-noise ratio multiplied by number of scans.

with the generalized mixed model is significant (p <.05). The outputs of statistical analysis with the generalized mixed model are shown in Table 4 (significance of individual factors and interactions among factors) and Figure 6 (visualization of effects). Because 10 ROIs were selected as regions activated by our task, and the resulting characteristics are very similar, the distribution of ROI metrics is shown only for two selected regions as examples. Figures 7 and 8 show the metrics and percent change of ME versus SE for the motor region (left precentral gyrus, ROI_ID = 1). Figures 9 and 10 show the same for the visual region (left middle occipital gyrus, ROI_ID = 6). The consistence of the observed effect across the regions is visible from Figure 6 (third column for the effect of the SE/ME data; fourth column for the effect of acquisition). It is clear that the effect of the ME data versus the SE data is consistent in the sense of the direction of the effect, and the regions differ mainly in the amplitude of effects (in some regions, the difference between SE and ME is smaller; in other regions, the difference is more pronounced). For the effect of the MB factor (fourth column in Figure 6), there is also clear consistency, even if few exceptions are visible.

General observations are that the ME data provides more suprathreshold voxels (ranging from negligible changes in runs 1 and 2 up to 64% in run 7), higher t-statistics (approximately from 1 to 30%), lower residuals (from 20 to 60%), higher activation SNR (from 1 to 70%), and lower estimated beta and PSC (about 10 to 15%). While the effects of beta and PSC are not significantly affected by acquisition parameters (the percentage of the decrease of beta and of PSC in the ME data was similar for all runs), the effects of t-statistics, residuals, and the number of suprathreshold voxels differ across runs. PSC is the only metric not significantly affected by the decrease of flip angle factor. But the general effect of flip angle is only the change of signal magnitude, and it does not interact with the factor ME (SE vs. ME) except in the variance of residuals. The variance of residuals is the metric most affected by flip angle, as well as the MB factor. The homogeneity of regions is expressed with the average correlation coefficient of the ROI representative signal with all the voxels in the region. The ME data improve the homogeneity for all runs and the effect is higher for more accelerated data. Practically, it means that ME can partially compensate for the decrease of homogeneity caused by higher acceleration. Beta values and PSC (which provides a very similar but standardized view on the BOLD signal change fitted with the GLM) are the only two metrics in which ME results are worse than SE results. Optimally combined ME data provides about 10% lower PSC than SE data. Mean t-value in 50 voxels around the activation peak and the number of suprathreshold voxels in the whole region indicate the advantage of slice acceleration with MBF = 4 and MBF = 6 because these values are better than unaccelerated data and the difference between SE and ME data is more pronounced here (approx. 20% higher t-values and 30% more suprathreshold voxels). On the other hand, acceleration with MBF = 8 provides worse results than lower MB factors as well as than unaccelerated data. Residual variance, regional homogeneity, and SNR show monotonic decreases with respect to increase of slice acceleration. The effects of flip angles on two selected ROIs (percent effect of decreased flip angle together with p-value of post-hoc test) are presented in Table S3.

4 | DISCUSSION

This study compared the results from SE fMRI data and ME fMRI data in seven runs with different acquisition parameters, specifically MB factors (i.e., various levels of slice acceleration) accompanied with two levels of flip angles. The aim was to better understand the relationship between the ME approach and various acquisition protocols, especially various levels of slice acceleration. A further partial aim, based on more general knowledge, was to find a suitable compromise between acquisition speed and final data quality. We intended to significantly extend the comparisons between ME and SE with accelerated data provided by previous studies. We bring a set of new

TABLE 4 Results from generalized mixed effect models assessing the factors of SE versus ME, slice accelerations (MB factor), flip angles (higher vs. lower), and individual ROI (ROI_ID 1–10)

Metric	Signific. of factor ME	Signific. of factor MBF	Signific. of factor FA	Signific. of factor ROI	Signific. of interaction ME × MBF	Signific. of interaction ME × FA	Signific. of interaction ME × ROI	Signific. of interaction MBF × FA	Signific. of interaction MBF × ROI	Signific. of interaction FA × ROI
Homogeneity	<.001	<.001	<.001	<.001	.251	.078	<.001	<.001	<.001	.215
Active voxels	<.001	<.001	<.001	<.001	<.001	.465	<.001	.188	<.001	.048
Residuals50	<.001	<.001	<.001	<.001	<.001	<.001	<.001	<.001	<.001	<.001
Meant50	<.001	<.001	<.001	<.001	<.001	.407	<.001	.001	<.001	.146
SNR50	.016	<.001	<.001	<.001	.099	.685	.901	.035	<.001	.657
PSC50	<.001	<.001	.194	<.001	.925	.967	<.001	.028	<.001	.863
Beta50	<.001	<.001	.001	<.001	.602	.614	<.001	.001	<.001	.129

Note: The values in the table represent the significance (*p*-value) of each individual factor or interaction between factors for each ROI metric. Abbreviations used in the table: FA, flip angle; ME, multi-echo; MBF, multiband factor; PSC, percent signal change of BOLD response estimated with general linear model; SNR, signal-to-noise ratio based on the BOLD response estimated with general linear model versus *SD* of residual.

information and more complex views on the interaction of ME fMRI with acquisition protocols. A few studies have combined ME MB acquisition at 7T (Boyacioğlu et al., 2015; Puckett et al., 2018). Several articles have concerned MEMB at 3T (Amemiya et al., 2019; Cohen et al., 2020, 2021; Olafsson et al., 2015). These articles compared only one single-band (slice unaccelerated) and one multi-band run. We tried to evaluate a broader range of acquisition settings differing in slice acceleration levels (MB factor) and flip angles and to assess ME advantages with a wide range of metrics that can provide a more general view on this topic. We chose the acquisition of ME data and the subsequent processing of the individual (middle) echo or of all echoes combined according to BOLD CNR (as a combination of calculated tSNR and TE). This approach has the advantage of analyzing the same time period, in contrast to independent measurements of SE fMRI data and ME data in two runs. This approach was used in a study by Amemiya et al. (2019). Cohen et al. (2020, 2021) used the acquisition of two independent runs for SE and ME data, which made it possible to optimize SE acquisition and reach a slightly lower TR. Our approach enabled us to measure more functional runs during one visit and therefore to test various acquisition settings—different levels of MB acceleration combined with different flip angles for the same MB-factor. Gonzalez-Castillo et al. (2011) observed that fMRI sequences with low flip angles provide the same BOLD percent signal change as for the Ernst angle, even if the signal level is decreased. This was tested using the same TR and without changes in the acquisition acceleration. For this reason, we used three pairs of sequences with the same parameters except for flip angle; we intended to verify whether their observation was true, especially for SE and ME data analysis. Flip angle was selected as a slightly rounded-down Ernst angle for odd runs and the flip angle from a higher acceleration level for even runs. The seventh sequence was not in a pair because of the high MB factor and low TR; reduction of the flip angle by more than 20° would obviously lead to unacceptable data quality and it does not make sense to try measure data with higher acceleration.

We selected several global and local metrics to evaluate our data to provide a complex view on the effects of ME data and accelerated acquisitions. One global metric used in our study was tSNR, in a modification suggested by Smith et al. (2013) for the Human Connectome Project. In this modification, standard tSNR is multiplied by the square root of the number of volumes measured in a specific functional run. This incorporates the statistical power of more time points provided by accelerated acquisition. Otherwise, any acceleration produces a decrease of tSNR because of the decrease of the measured signal. We calculated tSNR on a voxel-wise basis; subsequently, the mean tSNR was obtained for gray matter and white matter. The latter offers a more general overview of the time-series stability because white matter is not supposed to contain a significant portion of neuronal fluctuations. The gray matter contains fluctuations of artificial origin combined with neuronal resting-state fluctuations and task-induced fluctuations. Thus, the tSNR calculation in gray matter can be influenced by these signals of neuronal origin, even if we do not suppose that the task-induced fluctuations can significantly change the mean tSNR from the whole gray matter. The number of

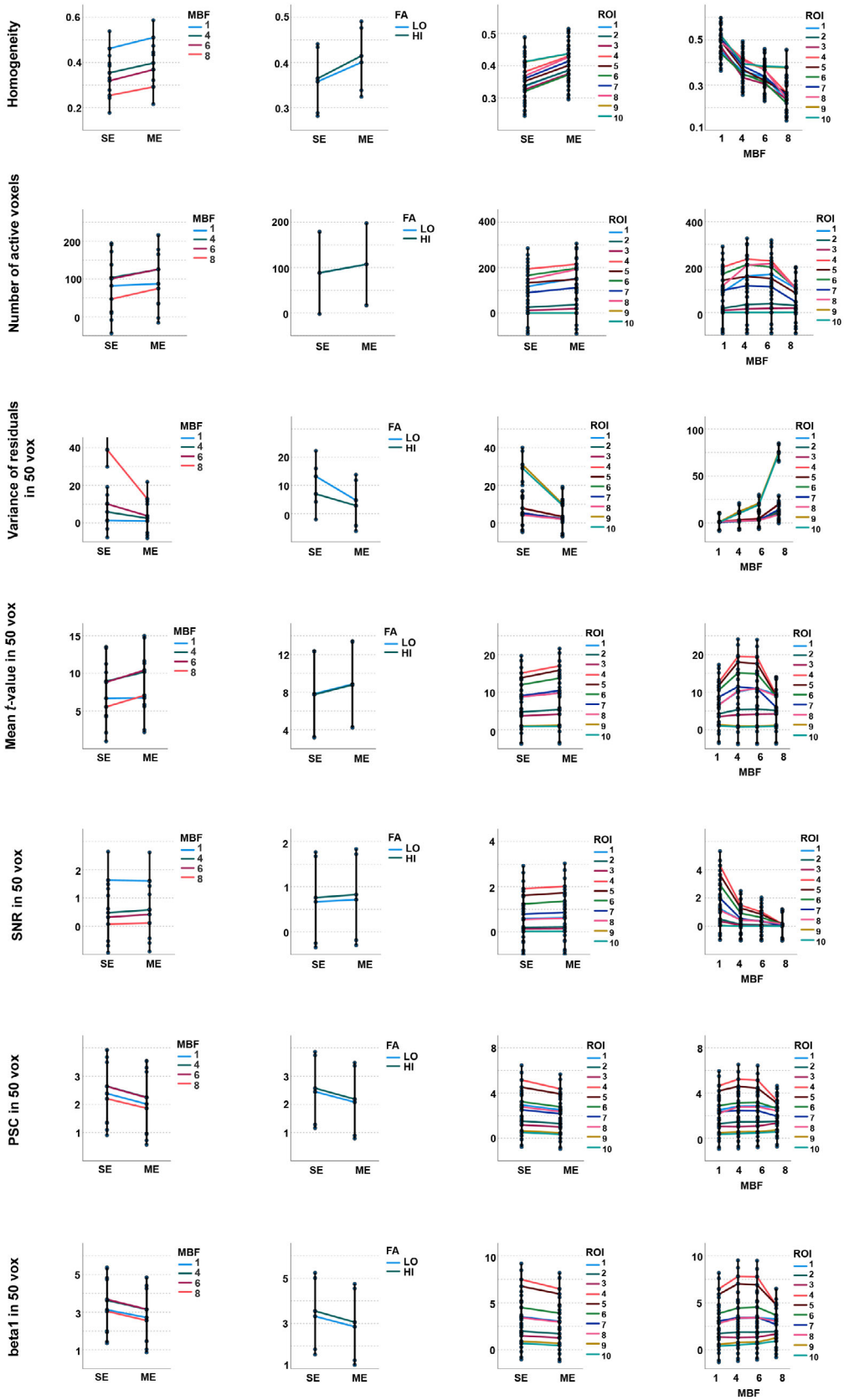

FIGURE 6 Overview of the effect of modeled factors in generalized mixed model statistics for local metrics (calculated in individual ROIs). Each row represents one metric (depicted on the left side). Estimated means (dots connected with lines) and 95% confidence intervals (whiskers) are presented for four types of graphs. First shows the effect of ME data on the metric for individual multi-band factors. Second shows the effect of ME data on the metric for two levels of flip angles (high or low angle). Third type shows the effect of ME data on the metric for individual region. Fourth type shows the effect of multi-band factor on the metric for individual region. FA, flip angle; GM, gray matter; MBF, multi-band factor; ME, optimally combined multi-echo data; ROI, region of interest; SE, single echo data; WM, white matter

suprathreshold voxels represents a measure of sensitivity and it is important to assess the basic activation results. The SNS metric (Shirer et al., 2015) can be interpreted as a signal-to-noise ratio for functional connectivity analysis because it is based on the distance (expressed by a *t*-test) between meaningful correlations among brain regions belonging to known functional networks and nonsense

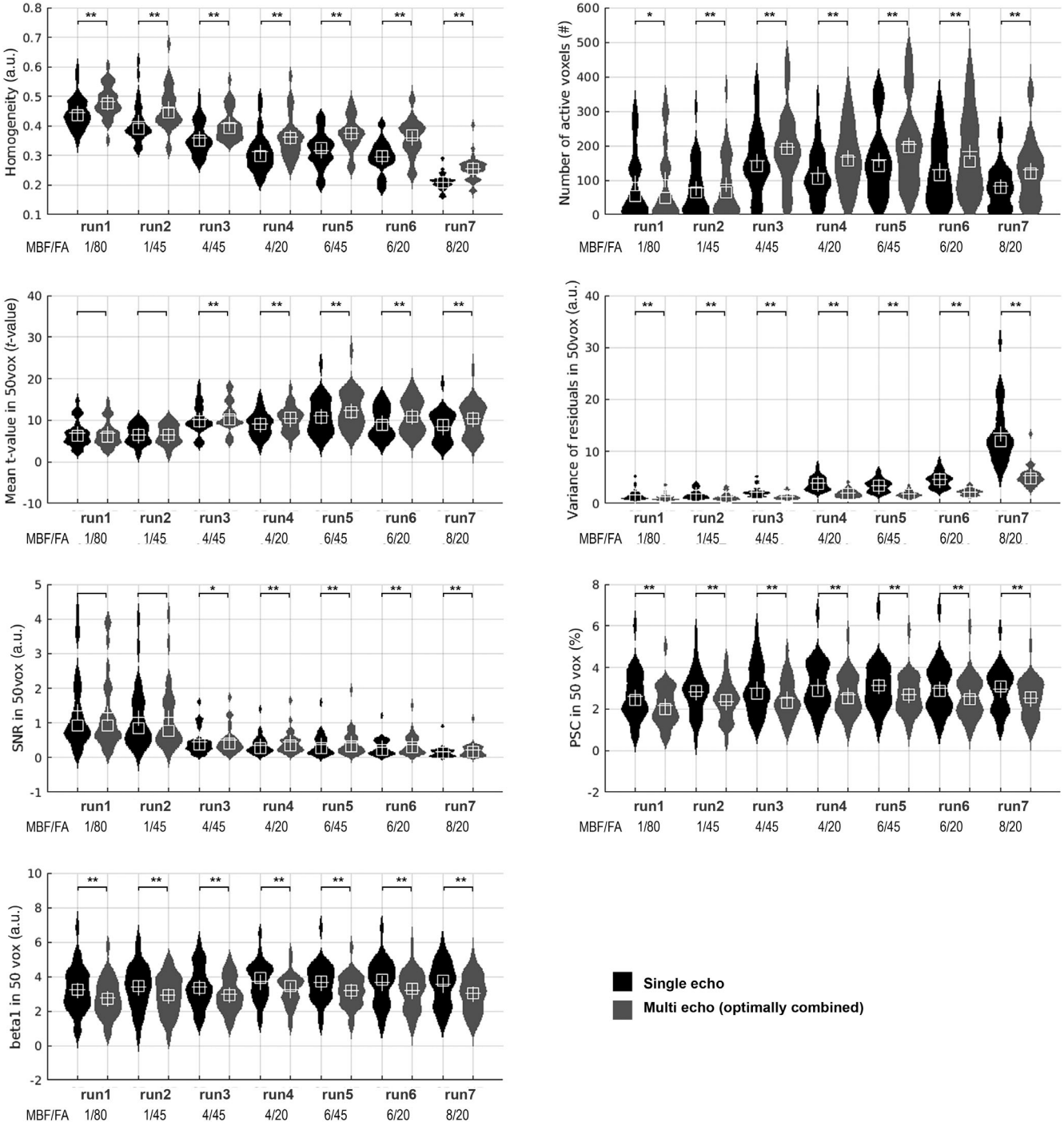

FIGURE 7 Distribution plots of local metrics from left precentral gyrus (ROI_1) for SE (black) and ME data (gray). White box represent median, white cross represents the mean of the distribution. Multi-band factors and flip angle values are given under the *x*-axis for each run. Significance of post-hot test (comparing SE and ME data from the same run) is depicted with stars above the distribution plots. *corresponds to p <.05 uncorrected. **corresponds to p <.05 corrected for number of runs. FA, flip angle; GM, gray matter; MBF, multi-band factor; ME, optimally combined multi-echo data; SE, single echo data; WM, white matter

correlations among brain regions and background noise (dark regions outside the brain). One may argue that SNS is more suitable for resting-state data than for task fMRI. But only a very small amount of gray matter is affected by task-induced activation, and the resting-state fluctuations are still present in the task data, which makes it possible to provide at least an approximation of the effect of ME on connectivity-based quality measures. Moreover, task-fMRI data is also analyzed with various connectivity methods—typically effective connectivity; therefore, this type of metric can be useful. Another critique of the SNS metric can be the calculation of correlations based on data

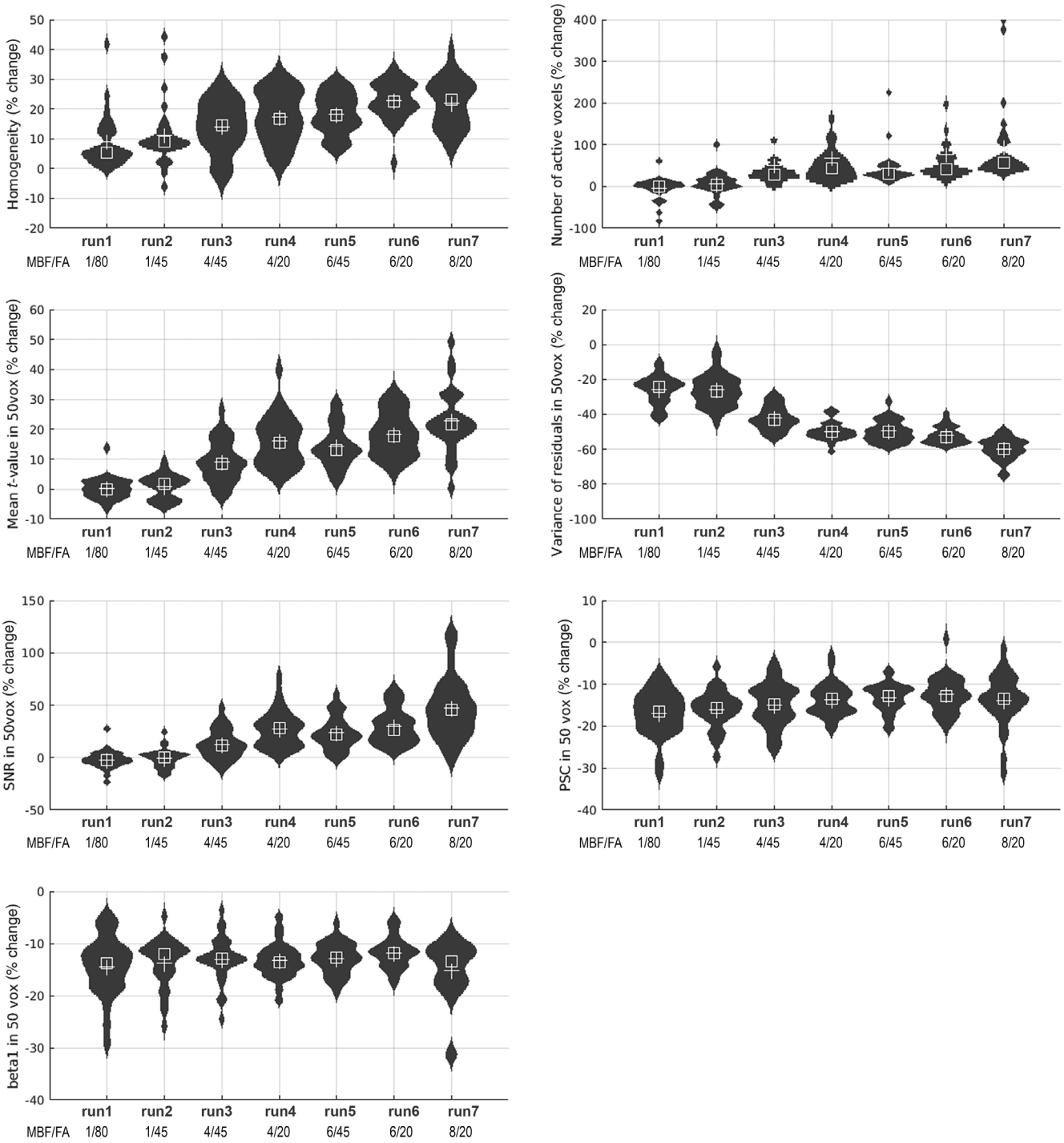

FIGURE 8 Distribution plots of the percent change between SE and ME local metrics (positive number corresponds to increase of metric for ME data) from left precentral gyrus (ROI_1). White box represent median, white cross represents the mean of the distribution. Multi-band factors and flip angle values are given under the *x*-axis for each run. FA, flip angle; GM, gray matter; MBF, multi-band factor; ME, optimally combined multi-echo data; SE, single echo data; WM, white matter

outside the brain. In an ideal case, data outside brain can contain thermal noise. Practically all artifacts spread across the k-space affect the data outside of the measured object. This can make violations of assumptions, but it can be taken into the consideration as meaningful behavior because all such widespread artifacts, such as leakage in slice acceleration techniques, head movements, and so on, decrease the SNS metric, which is a warning that the analysis of connectivity can be affected by artifacts.

Smoothness is another measure of general data quality used in the quality control pipeline, such as in the Human Connectome Project (Marcus et al., 2013). A decrease of smoothness can be caused by the presence of image noise and image artifacts with higher spatial

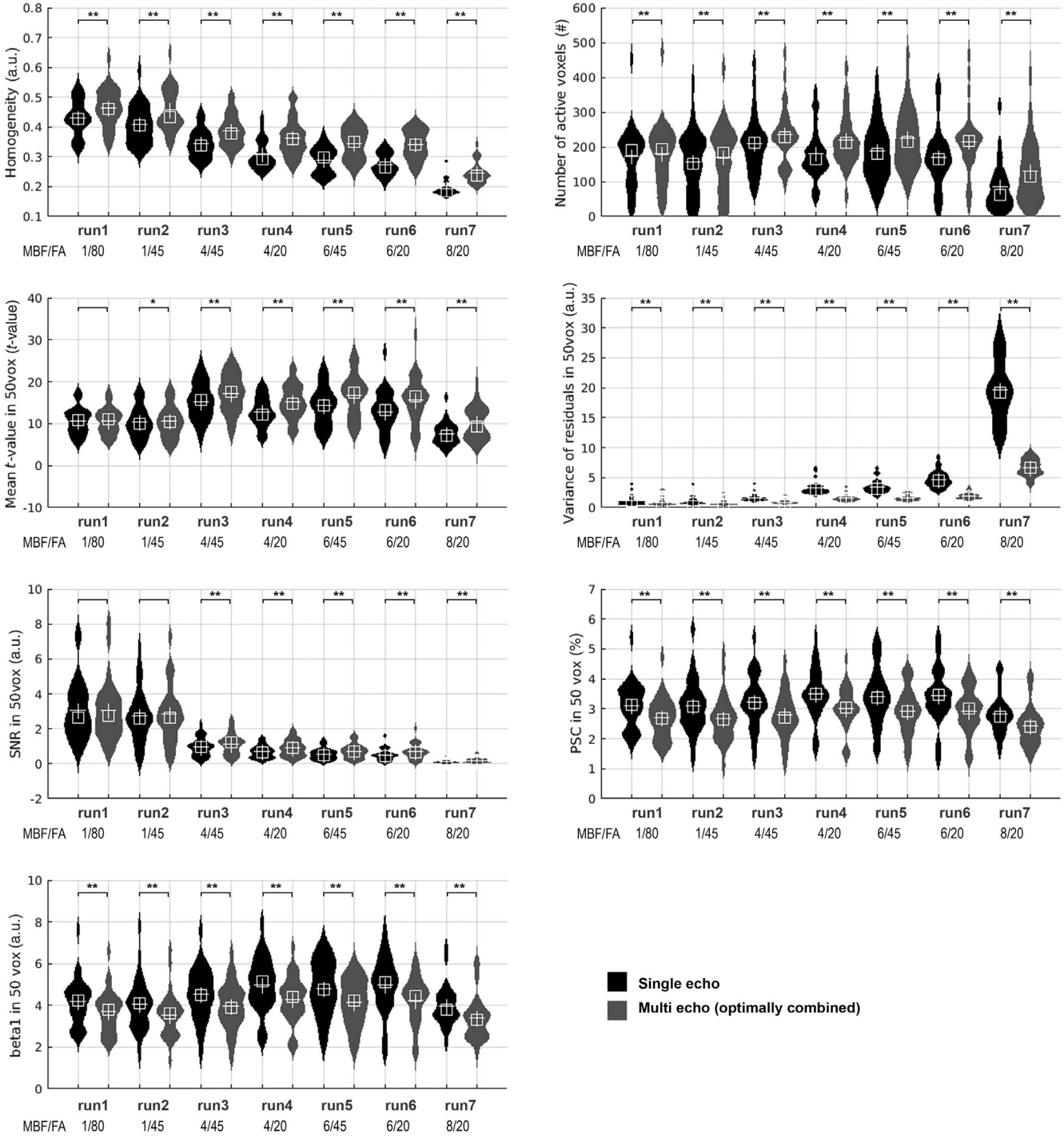

FIGURE 9 Distribution plots of local metrics from left middle occipital gyrus (ROI_6) for SE (black) and ME data (gray). White box represent median, white cross represents the mean of the distribution. Multi-band factors and flip angle values are given under the *x*-axis for each run. Significance of post-hot test (comparing SE and ME data from the same run) is depicted with stars above the distribution plots. *corresponds to p <.05 uncorrected. **corresponds to p <.05 corrected for number of runs. FA, flip angle; GM, gray matter; MBF, multi-band factor; ME, optimally combined multi-echo data; SE, single echo data; WM, white matter

frequencies. On the other hand, some types of artifacts like movement can increase the smoothness of the data because of image blurring; thus, the metric has to be interpreted carefully. We did not observe any outliers and unexpected changes in smoothness. The global gray matter average of residual variance after GLM fitting is another useful metric because it provides the amount of unexplained signals and an estimate of the global noise levels in measured data. The last two global metrics, path length and node strength, are taken from global graph metrics calculated from the adjacency matrix of functional connectivity. In a study concerning the quality of

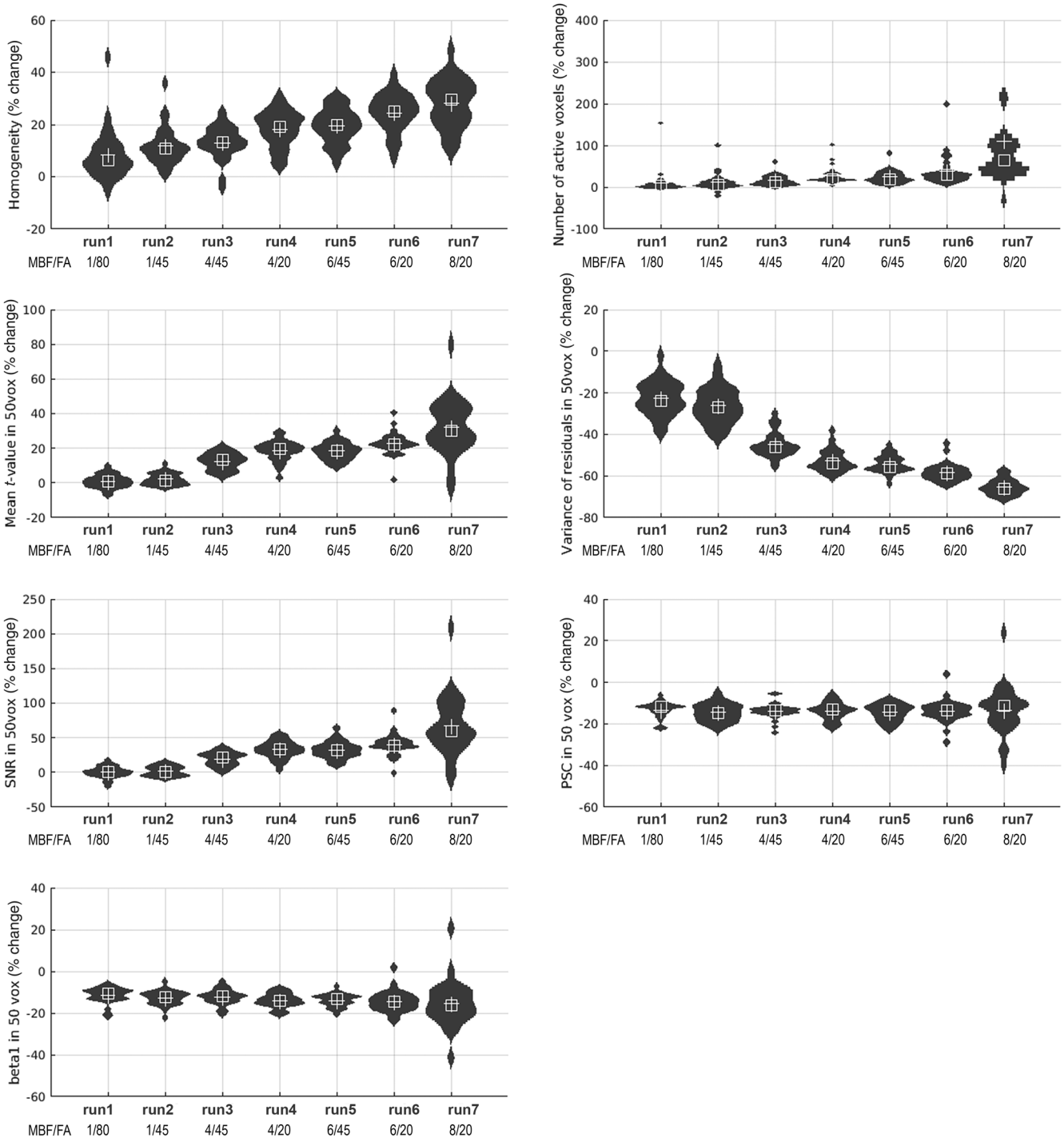

FIGURE 10 Distribution plots of the percent change between SE and ME local metrics (positive number corresponds to increase of metric for ME data) from left middle occipital gyrus (ROI_6). White box represent median, white cross represents the mean of the distribution. Multi-band factors and flip angle values are given under the *x*-axis for each run. FA, flip angle; GM, gray matter; MBF, multi-band factor; ME, optimally combined multi-echo data; SE, single echo data; WM, white matter

representative signals from atlas-based ROIs for functional connectivity (Gajdoš et al., 2018), these two metrics showed clear changes for noisy representative signals. Decreasing node strength and increasing path length cause the network to become more random. Thus, our hypothesis was that we can observe these effects for more accelerated data (given by image quality decrease) and ME data can offer improvements in this deviation from unaccelerated results. These two metrics are part of the analysis of functional connectivity, but we believe they provide, like SNS, a meaningful extension of task-based activation metrics and are valid even for task data. We expected that higher data quality is represented by higher tSNR, higher SNS, higher smoothness (even if this should be

interpreted carefully), higher number of active voxels, and lower residual variance.

As local metrics, we used the parameters obtained directly from the GLM (*t*-statistics, beta values, and residuals) or advanced metrics (BOLD activation SNR, percent signal change, and mean correlation of representative signals with all the voxels in the region) but calculated in selected AAL regions containing activation in our visual-motor task. Two metrics were based on whole AAL regions—the number of suprathreshold voxels and the mean correlation of the representative signal with all the voxels in the region, which represents the measure of homogeneity in the region. Other local metrics were calculated from the 50 most significant voxels around the peak activation in the region. This made it possible to avoid averaging possible task-anticorrelated or just noisy voxels together with the task-activated voxels because some AAL regions are much larger than the extent of task activation. This could also be overcome using ROIs based directly on activation, but we wanted to avoid circularity and favor some run or SE/ME model. We also calculated mentioned metrics as averages from complete AAL regions, and the characteristics were close to the presented ones. We did not include this data in this article, because it does not provide additional information. We expected that higher data quality in ROIs is expressed with higher number of active voxels, higher *t*-values, higher homogeneity of region, higher activation SNR and lower residual variance.

All metrics (except for the beta values and corresponding PSC, discussed later) showed significant improvement for the ME data over the SE data. This was more pronounced in runs with accelerated acquisition. The practical improvement of metrics was typically by a few percent for unaccelerated data, but the effect size (improvement of ME vs. SE) increased in accelerated data up to 70%. The interaction between the factors of SE/ME model and MBF was significant for most of the global metrics, except SNS and node strength, and some of local metrics, specifically number of suprathreshold voxels, residual variance, and mean t-value. This means that the ME approach provides even more benefits for highly accelerated data.

Acquisition settings affect the measured data despite the SE or ME variant (see Figures 3–10, Tables 3 and 4). All metrics are significantly affected by the MB factor, but while some metrics decrease or increase with the MB factor in a monotonic way, and thus do not provide easy answers about optimal acceleration, several metrics show more interesting behavior. These are the tSNRn in gray matter, tSNRn in white matter, the number of suprathreshold voxels in gray matter, the number of suprathreshold voxel in ROIs, mean *t*-value in ROIs, and partially also PSC in ROIs. The MB factors of 4 and 6 provide better results than unaccelerated data and better than the MB factor of 8. This suggests that such intermediate (MBF = 4) or upper intermediate (MBF = 6) levels of slice acceleration are optimal for ME data. Unfortunately, we are not able to evaluate mild slice acceleration (e.g., an MB factor of 2) because this was not included in our dataset. An important note is that in our dataset, as in many ME datasets, slice acceleration was combined with a GRAPPA Parallel Acquisition Techniques (PAT) factor of 2, because it is necessary to decrease the echo train length to measure several echoes within a reasonable TR. Practically, our accelerations were 4 × 2, 6 × 2, and 8 × 2. For this reason, MBF = 8 in our dataset showed a dramatic decrease in data quality, while acquisition with MBF = 8 without the PAT factor (e.g., as used in Human Connectome Project fMRI) provided acceptable data.

We expected that PSC, betas, and *t*-values would not be not affected by flip angle decrease, according to the results of Gonzalez-Castillo et al. (2011) indicating that lower flip angles do not affect data sensitivity. But the flip angle factor was significant for all task activation-based metrics compared with the generalized mixed model, except for the PSC metric. This might be explained by the fact that the statistical model assessed a large number of very small differences. For instance, concerning *t*-values and betas in ROIs, a post hoc paired *t*-test revealed only a few significant differences across the ROIs and runs. Residual variance is the metric most affected by lower flip angles, especially for the mid acceleration. This may be caused by decreasing amounts of physiological noise in fMRI data, as was reported by Gonzalez-Castillo et al. (2011), but a detailed explanation of this phenomenon is beyond the scope of this article.

Our results are in agreement with previous articles introducing ME fMRI acquisition (Amemiya et al., 2019; Cohen et al., 2020, 2021; Kundu et al., 2012, 2017; Olafsson et al., 2015; Poser et al., 2006), but we extended and verified the results for accelerated data with middle and higher MB factors (4–8). Although the improvement caused by optimally combined ME data is present even for very high acceleration (MB factor of 8 in run 7), we do not recommend measuring such highly accelerated fMRI data because the loss of data quality compared to run1 is really huge, as can be seen with the tSNRn metric; we used a modified version of tSNR according Smith et al. (2013) that takes into consideration the number of measured timepoints as a key parameter for statistical power.

Concerning group-level activation, the patterns seemed to be similar and the main differences (large number of active voxels) with ME were observed in the basal ganglia, which is in concordance with the findings by Puckett et al. (2018).

As we stated earlier, beta values and PSC in were lower in the ME model than in the SE model. This is caused by a combination of data from individual echoes. In the current implementation of weighted averages (Poser et al., 2006), the weights are given by the multiplication of tSNR in each individual voxel and TE. The first one should favor data with a higher signal mean and lower signal variance, that is, typically data from the first echo. The second member represents the sensitivity to the BOLD response. Unfortunately, even in regions that are not affected by signal dropouts, the first echo can play a more important role than the later ones and, in this case, the weighted average provides slightly lower BOLD PSC than for the individual middle echo. Because all other parameters (both local and global) are better for the ME model, we do not consider this a serious problem. It can raise the question of whether CNR-based weighting is the best possible solution, but comprehensive (complex) research on new weighting is beyond the scope of this article. Similar findings were described in previous studies (Cohen et al., 2020; Gonzalez-Castillo et al., 2016; Heunis et al., 2021).

We did not address the effect of data cleaning during post-processing (various type of filtering, regression), because this would add more factors to the final analysis and interpretation. In our data processing pipeline, only movement regression was used, with an extended set of 24 parameters (Friston et al., 1996). We did not regress out signals from white matter or cerebral-spinal-fluid compartments because previous studies reported this should be considered carefully for task data (Bartoň et al., 2019).

5 | CONCLUSION

The results of this study clearly show the benefits of the ME approach for fast fMRI acquisition. This phenomenon was verified by all the evaluated metrics: group activation maps, global metrics, and detailed analysis of selected ROIs. The increase in signal quality was proven to be statistically significant compared to standard SE acquisition.

Generally, ME acquisition is meaningful and useful for fast imaging, where it can improve the data quality over the SE approach. By averaging three TEs, it is possible to eliminate noise and motion artifacts to some extent and to obtain higher signal values. In our measurements, this principle applied to all of the accelerated runs, although we do not recommend the last one (run 7) for routine use because the quality of acquired data is very low. We suggest using a MB factor in the range of 4–6 as a safe option when combined with a PAT factor of 2 for acquisition of ME data.

ACKNOWLEDGMENTS

The work was supported from the European Regional Development Fund project "National infrastructure for biological and medical imaging" (No. CZ.02.1.01/0.0/0.0/16_013/0001775). The authors acknowledge the core facility MAFIL of CEITEC supported by the Czech-BioImaging large RI project (LM2015062 and LM2018129 funded by MEYS CR) for their support in obtaining the scientific data presented in this article. Many thanks to Anne Johnson for proofreading.

CONFLICT OF INTEREST

The authors declare no potential conflict of interest.

DATA AVAILABILITY STATEMENT

The data that support the findings of this study are available from the corresponding author upon reasonable request.

ORCID

Anežka Kovářová https://orcid.org/0000-0001-6552-8066
Martin Gajdoš https://orcid.org/0000-0003-2780-7472
Ivan Rektor https://orcid.org/0000-0002-9635-7404
Michal Mikl https://orcid.org/0000-0003-1190-346X

REFERENCES

Amemiya, S., Yamashita, H., Takao, H., & Abe, O. (2019). Integrated multi-echo denoising strategy improves identification of inherent language laterality. *Magnetic Resonance in Medicine*, *81*(5), 3262–3271. https://doi.org/10.1002/mrm.27620

Bartoň, M., Mareček, R., Krajčovičová, L., Slavíček, T., Kašpárek, T., Zemánková, P., … Mikl, M. (2019). Evaluation of different cerebrospinal fluid and white matter fMRI filtering strategies—Quantifying noise removal and neural signal preservation. *Human Brain Mapping*, *40*(4), 1114–1138. https://doi.org/10.1002/hbm.24433

Boyacioğlu, R., Schulz, J., Koopmans, P. J., Barth, M., & Norris, D. G. (2015). Improved sensitivity and specificity for resting state and task fMRI with multiband multi-echo EPI compared to multi-echo EPI at 7T. *NeuroImage*, *119*, 352–361. https://doi.org/10.1016/j.neuroimage.2015.06.089

Chen, L., Vu, A. T., Xu, J., Moeller, S., Ugurbil, K., Yacoub, E., & Feinberg, D. A. (2015). Evaluation of highly accelerated simultaneous multi-slice EPI for fMRI. *NeuroImage*, *104*, 452–459. https://doi.org/10.1016/j.neuroimage.2014.10.027

Cohen, A. D., Jagra, A. S., Yang, B., Fernandez, B., Banerjee, S., & Wang, Y. (2020). Detecting task functional MRI activation using the multiband multiecho (MBME) echo-planar imaging (EPI) sequence. *Journal of Magnetic Resonance Imaging*, *53*, 1366–1374. https://doi.org/10.1002/jmri.27448

Cohen, A. D., Nencka, A. S., Marc Lebel, R., & Wang, Y. (2017). Multiband multi-echo imaging of simultaneous oxygenation and flow timeseries for resting state connectivity. *PLoS One*, *12*(3), 1–23. https://doi.org/10.1371/journal.pone.0169253

Cohen, A. D., Yang, B., Fernandez, B., Banerjee, S., & Wang, Y. (2021). Improved resting state functional connectivity sensitivity and reproducibility using a multiband multi-echo acquisition. *NeuroImage*, *225*-(April 2020), 117461. https://doi.org/10.1016/j.neuroimage.2020.117461

Demetriou, L., Kowalczyk, O. S., Tyson, G., Bello, T., Newbould, R. D., & Wall, M. B. (2018). A comprehensive evaluation of increasing temporal resolution with multiband-accelerated protocols and effects on statistical outcome measures in fMRI. *NeuroImage*, *176*(April), 404–416. https://doi.org/10.1016/j.neuroimage.2018.05.011

Feinberg, D. A., & Setsompop, K. (2013). Ultra-fast MRI of the human brain with simultaneous multi-slice imaging. *Journal of Magnetic Resonance*, *229*, 90–100. https://doi.org/10.1016/j.jmr.2013.02.002

Fernandez, B., Leuchs, L., Sämann, P. G., Czisch, M., & Spoormaker, V. I. (2017). Multi-echo EPI of human fear conditioning reveals improved BOLD detection in ventromedial prefrontal cortex. *NeuroImage*, *156*-(November 2016), 65–77. https://doi.org/10.1016/j.neuroimage.2017.05.005

Friston, K. J., Williams, S., Howard, R., Frackowiak, R. S. J., & Turner, R. (1996). Movement-related effects in fMRI time-series. *Magnetic Resonance in Medicine*, *35*(3), 346–355. https://doi.org/10.1002/mrm.1910350312

Gajdoš, M., Mikl, M., & Mareček, R. (2016). Mask_explorer: A tool for exploring brain masks in fMRI group analysis. *Computer Methods and Programs in Biomedicine*, *134*, 155–163. https://doi.org/10.1016/J.CMPB.2016.07.015

Gajdoš, M., Výtvarová, E., Fousek, J., Lamoš, M., & Mikl, M. (2018). Robustness of representative signals relative to data loss using atlas-based parcellations. *Brain Topography*, *31*, 767–779. https://doi.org/10.1007/s10548-018-0647-6

Gonzalez-Castillo, J., Panwar, P., Buchanan, L. C., Caballero-Gaudes, C., Handwerker, D. A., Jangraw, D. C., … Bandettini, P. A. (2016). Evaluation of multi-echo ICA denoising for task based fMRI studies: Block designs, rapid event-related designs, and cardiac-gated fMRI. *NeuroImage*, *141*, 452–468. https://doi.org/10.1016/j.neuroimage.2016.07.049

Gonzalez-Castillo, J., Roopchansingh, V., Bandettini, P. A., & Bodurka, J. (2011). Physiological noise effects on the flip angle selection in BOLD fMRI. *NeuroImage*, *54*(4), 2764–2778. https://doi.org/10.1016/j.neuroimage.2010.11.020

Griswold, M. A., Jakob, P. M., Heidemann, R. M., Nittka, M., Jellus, V., Wang, J., … Haase, A. (2002). Generalized autocalibrating partially parallel acquisitions (GRAPPA). *Magnetic Resonance in Medicine*, *47*(6), 1202–1210. https://doi.org/10.1002/mrm.10171

Hamilton, J., Franson, D., & Seiberlich, N. (2017). Recent advances in parallel imaging for MRI. *Progress in Nuclear Magnetic Resonance Spectroscopy*, *101*, 71–95. https://doi.org/10.1016/j.pnmrs.2017.04.002

Heunis, S., Breeuwer, M., Caballero-Gaudes, C., Hellrung, L., Huijbers, W., Jansen, J. F., … Aldenkamp, A. P. (2021). The effects of multi-echo fMRI combination and rapid T2*-mapping on offline and real-time BOLD sensitivity. *NeuroImage*, *238*, 118244. https://doi.org/10.1016/J.NEUROIMAGE.2021.118244

Krüger, G., & Glover, G. H. (2001). Physiological noise in oxygenation-sensitive magnetic resonance imaging. *Magnetic Resonance in Medicine*, *46*(4), 631–637. https://doi.org/10.1002/mrm.1240

Kundu, P., Brenowitz, N. D., Voon, V., Worbe, Y., Vértes, P. E., Inati, S. J., … Bullmore, E. T. (2013). Integrated strategy for improving functional connectivity mapping using multiecho fMRI. *Proceedings of the National Academy of Sciences of the United States of America*, *110*(40), 16187–16192. https://doi.org/10.1073/pnas.1301725110

Kundu, P., Inati, S. J., Evans, J. W., Luh, W. M., & Bandettini, P. A. (2012). Differentiating BOLD and non-BOLD signals in fMRI time series using multi-echo EPI. *NeuroImage*, *60*(3), 1759–1770. https://doi.org/10.1016/j.neuroimage.2011.12.028

Kundu, P., Voon, V., Balchandani, P., Lombardo, M. V., Poser, B. A., & Bandettini, P. A. (2017). Multi-echo fMRI: A review of applications in fMRI denoising and analysis of BOLD signals. *NeuroImage*, *154*(March), 59–80. https://doi.org/10.1016/j.neuroimage.2017.03.033

Luo, W. L., & Nichols, T. E. (2003). Diagnosis and exploration of massively univariate neuroimaging models. *NeuroImage*, *19*(3), 1014–1032. https://doi.org/10.1016/S1053-8119(03)00149-6

Marcus, D. S., Harms, M. P., Snyder, A. Z., Jenkinson, M., Wilson, J. A., Glasser, M. F., … Van Essen, D. C. (2013). Human Connectome Project informatics: Quality control, database services, and data visualization. *NeuroImage*, *80*, 202–219. https://doi.org/10.1016/j.neuroimage.2013.05.077

McDowell, A. R., & Carmichael, D. W. (2019). Optimal repetition time reduction for single subject event-related functional magnetic resonance imaging. *Magnetic Resonance in Medicine*, *81*(3), 1890–1897. https://doi.org/10.1002/mrm.27498

Ogawa, S., Lee, T. M., Kay, A. R., & Tank, D. W. (1990). Brain magnetic-resonance-imaging with contrast dependent on blood oxygenation. *Proceedings of the National Academy of Sciences of the United States of America*, *87*(24), 9868–9872. https://doi.org/10.1073/pnas.87.24.9868

Olafsson, V., Kundu, P., Wong, E. C., Bandettini, P. A., & Liu, T. T. (2015). Enhanced identification of BOLD-like components with multi-echo simultaneous multi-slice (MESMS) fMRI and multi-echo ICA. *NeuroImage*, *112*, 43–51. https://doi.org/10.1016/j.neuroimage.2015.02.052

Poser, B. A., Versluis, M. J., Hoogduin, J. M., & Norris, D. G. (2006). BOLD contrast sensitivity enhancement and artifact reduction with multi-echo EPI: Parallel-acquired inhomogeneity-desensitized fMRI. *Magnetic Resonance in Medicine*, *55*(6), 1227–1235. https://doi.org/10.1002/mrm.20900

Posse, S., Wiese, S., Gembris, D., Mathiak, K., Kessler, C., Grosse-Ruyken, M. L., … Kiselev, V. G. (1999). Enhancement of BOLD-contrast sensitivity by single-shot multi-echo functional MR imaging. *Magnetic Resonance in Medicine*, *42*(1), 87–97. https://doi.org/10.1002/(SICI)1522-2594(199907)42:1<87::AID-MRM13>3.0.CO;2-O

Power, J. D., Barnes, K. A., Snyder, A. Z., Schlaggar, B. L., & Petersen, S. E. (2012). Spurious but systematic correlations in functional connectivity MRI networks arise from subject motion. *NeuroImage*, *59*(3), 2142–2154. https://doi.org/10.1016/j.neuroimage.2011.10.018

Pruessmann, K. P., Weiger, M., Scheidegger, M. B., & Boesiger, P. (1999). SENSE: Sensitivity encoding for fast MRI. *Magnetic Resonance in Medicine*, *42*(5), 952–962. https://doi.org/10.1002/(SICI)1522-2594(199911)42:5<952::AID-MRM16>3.0.CO;2-S

Puckett, A. M., Bollmann, S., Poser, B. A., Palmer, J., Barth, M., & Cunnington, R. (2018). Using multi-echo simultaneous multi-slice (SMS) EPI to improve functional MRI of the subcortical nuclei of the basal ganglia at ultra-high field (7T). *NeuroImage*, *172*(November 2017), 886–895. https://doi.org/10.1016/j.neuroimage.2017.12.005

Sahib, A. K., Mathiak, K., Erb, M., Elshahabi, A., Klamer, S., Scheffler, K., … Ethofer, T. (2016). Effect of temporal resolution and serial autocorrelations in event-related functional MRI. *Magnetic Resonance in Medicine*, *76*(6), 1805–1813. https://doi.org/10.1002/mrm.26073

Setsompop, K., Gagoski, B. A., Polimeni, J. R., Witzel, T., Wedeen, V. J., & Wald, L. L. (2012). Blipped-controlled aliasing in parallel imaging for simultaneous multislice echo planar imaging with reduced g-factor penalty. *Magnetic Resonance in Medicine*, *67*(5), 1210–1224. https://doi.org/10.1002/mrm.23097

Shirer, W. R., Jiang, H., Price, C. M., Ng, B., & Greicius, M. D. (2015). Optimization of rs-fMRI pre-processing for enhanced signal-noise separation, test-retest reliability, and group discrimination. *NeuroImage*, *117*, 67–79. https://doi.org/10.1016/j.neuroimage.2015.05.015

Šimko, P., Pupíková, M., Gajdoš, M., & Rektorová, I. (2021). Cognitive aftereffects of acute tDCS coupled with cognitive training: An fMRI study in healthy seniors. *Neural Plasticity*, *2021*, 1–10. https://doi.org/10.1155/2021/6664479

Smith, S. M., Beckmann, C. F., Andersson, J. L. R., Auerbach, E. J., Bijsterbosch, J., Douaud, G., … Glasser, M. F. (2013). Resting-state fMRI in the Human Connectome Project for the WU-Minn HCP Consortium. *NeuroImage*, *80*, 144–168. https://doi.org/10.1016/j.neuroimage.2013.05.039

Todd, N., Moeller, S., Auerbach, E. J., Yacoub, E., Flandin, G., & Weiskopf, N. (2016). Evaluation of 2D multiband EPI imaging for high-resolution, whole-brain, task-based fMRI studies at 3T: Sensitivity and slice leakage artifacts. *NeuroImage*, *124*, 32–42. https://doi.org/10.1016/j.neuroimage.2015.08.056

Triantafyllou, C., Wald, L. L., & Hoge, R. D. (2011). Echo-time and field strength dependence of BOLD reactivity in veins and parenchyma using flow-normalized hypercapnic manipulation. *PLoS One*, *6*(9), e24519. https://doi.org/10.1371/journal.pone.0024519

Tzourio-Mazoyer, N., Landeau, B., Papathanassiou, D., Crivello, F., Etard, O., Delcroix, N., … Joliot, M. (2002). Automated anatomical labeling of activations in SPM using a macroscopic anatomical parcellation of the MNI MRI single-subject brain. *NeuroImage*, *15*(1), 273–289. https://doi.org/10.1006/nimg.2001.0978

SUPPORTING INFORMATION

Additional supporting information may be found in the online version of the article at the publisher's website.

How to cite this article: Kovářová, A., Gajdoš, M., Rektor, I., & Mikl, M. (2022). Contribution of the multi-echo approach in accelerated functional magnetic resonance imaging multiband acquisition. *Human Brain Mapping*, *43*(3), 955–973. https://doi.org/10.1002/hbm.25698